SCIENCE CHINA
Chemistry

•ARTICLES•

January 2019 Vol.62 No.1: 118–125
https://doi.org/10.1007/s11426-018-9373-0

High performance TiP_2O_7 nanoporous microsphere as anode material for aqueous lithium-ion batteries

Yunping Wen[1†], Yao Liu[1†], Duan Bin[1], Zhuo Wang[1], Congxiao Wang[1], Yuliang Cao[2], Xinping Ai[2] & Yongyao Xia[1*]

[1]*Collaborative Innovation Center of Chemistry for Energy Materials, Department of Chemistry, Shanghai Key Laboratory of Molecular Catalysis and Innovative Materials, Institute of New Energy, Fudan University, Shanghai 200433, China;*
[2]*Hubei Key Laboratory Electrochem Power Sources, College of Chemistry and Molecular Science, Wuhan University, Wuhan 430072, China*

Received July 13, 2018; accepted October 25, 2018; published online December 21, 2018

This work developed a facile way to mass-produce a carbon-coated TiP_2O_7 nanoporous microsphere (TPO-NMS) as anode material for aqueous lithium-ion batteries via solid-phase synthesis combined with spray drying method. TiP_2O_7 shows great prospect as anode for aqueous rechargeable lithium-ion batteries (ALIBs) in view of its appropriate intercalation potential of −0.6 V (vs. SCE) before hydrogen evolution in aqueous electrolytes. The resulting sample presents the morphology of secondary microspheres (ca. 20 μm) aggregated by carbon-coated primary nanoparticles (100 nm), in which the primary nanoparticles with uniform carbon coating and sophisticated pore structure greatly improve its electrochemical performance. Consequently, TPO-NMS delivers a reversible capacity of 90 mA h/g at 0.1 A/g, and displays enhanced rate performance and good cycling stability with capacity retention of 90% after 500 cycles at 0.2 A/g. A full cell containing TPO-NMS anode and $LiMn_2O_4$ cathode delivers a specific energy density of 63 W h/kg calculated on the total mass of anode and cathode. It also shows good rate capacity with 56% capacity maintained at 10 A/g rate (vs. 0.1 A/g), as well as long cycle life with the capacity retention of 82% after 1000 cycles at 0.5 A/g.

aqueous lithium-ion batteries, H_2 evolution reaction, anode, TiP_2O_7, spray drying

Citation: Wen Y, Liu Y, Bin D, Wang Z, Wang C, Cao Y, Ai X, Xia Y. High performance TiP_2O_7 nanoporous microsphere as anode material for aqueous lithium-ion batteries. *Sci China Chem*, 2019, 62: 118–125, https://doi.org/10.1007/s11426-018-9373-0

1 Introduction

With the concern of safety and green environmental protection, aqueous rechargeable lithium-ion batteries (ARLBs) have attracted much more attention as one of the most promising stationary energy sources [1–3]. ARLBs are expected not only to solve the security problem resulting from the use of toxic and flammable organic electrolytes in lithium-ion batteries, but also to display longer cycle life than those commercialized aqueous batteries (e.g. Ni-MH and lead-acid). Since the first aqueous cell $VO_2/LiMn_2O_4$ was reported by Dahn *et al*. in 1994 [4], many aqueous lithium-ion battery systems and technologies have been developed [5–8]. Generally, conventional lithium transition metal oxides widely used as cathodes for lithium-ion batteries, such as $LiMn_2O_4$ [9,10], $LiCoO_2$ [11,12] and $LiFePO_4$ [13,14], are qualified for ARLBs. In contrast, anode candidates for ARLBs are insufficient and their electrochemical properties, especially cycling stability are less than satisfactory, which can be ascribed to the narrow electrochemical window and unavoidable side reactions resulting from the introduction of aqueous electrolytes, such as the dissolution of electrode material, and the H_2/O_2 evolution reactions [15–17].

In order to solve these issues, various strategies including carbon coating and doped have been developed to improve

† These authors contributed equally to this work.
*Corresponding author (email: yyxia@fudan.edu.cn)

the stability of anode materials in aqueous electrolytes. As the first kind of anode for ARLBs, VO_2 and other vanadium-based compounds deeply suffer from the intrinsic solubility [4,18]. Since that, NASCION-type $LiTi_2(PO_4)_3$ with superior chemical stability has been proposed as an ideal substitute [15]. Luo *et al*. [16,17] reported carbon-coated $LiTi_2(PO_4)_3$ associated with oxygen elimination and pH adjustment showed much improved cycling performance. Although $LiTi_2(PO_4)_3$ is currently the most prospective anode material in ARLBs, its further application is restricted by the side reaction of hydrogen evolution. As reported, the intercalation potential of $LiTi_2(PO_4)_3$ is extremely close to the hydrogen evolution potential [1,7], the hydrogen evolution inevitably happens during the whole charge process, failing to use the full capacity of anode material before the decomposition of electrolyte [19]. In addition, the hydrogen evolution usually causes the change of the pH value in electrolytes, which definitely undermines the stability of anode material and leads to the rapid capacity loss of the whole battery [15]. Up to now, little progress has been made to tackle the primary concern of hydrogen evolution. Thus, to develop an advanced anode with proper intercalation potential before hydrogen evolution becomes a breakthrough.

With the reversible Ti^{4+}/Ti^{3+} redox couple at 2.6 V (vs. Li/Li^+, −0.6 V vs. SCE) before hydrogen evolution, titanium pyrophosphate (TiP_2O_7) shows huge potential as anode for ARLBs [20]. TiP_2O_7 has a cubic structure consisting of TiO_6 octahedra and P_2O_7 double-tetrahedra sharing corner. Such an open 3D network provides superior properties of chemical/thermal stability and fast Li-ion diffusion, rivalling the NASCION structure of $LiTi_2(PO_4)_3$ [20–23]. However, its relatively slow development as anode for ARLBs since firstly reported in 2007 [7] may be attributed to the following aspects: firstly, there is severe particles agglomeration for TiP_2O_7 during the synthesis process. Secondly, the inferior electronic conductivity restricts its electrochemical performance. Despite some enhancement has been achieved through effective strategies like carbon coating and particle downsizing in the last decade, there are lack of facile and effective synthesis methods to achieve the comprehensive optimization of the electrochemical performance of TiP_2O_7 [24–26].

Herein, we developed a facile way to fabricate carbon-coated TiP_2O_7 nanoporous microsphere (TPO-NMS) using solid-phase synthesis combined with spray drying method. The obtained composite was characterized by X-ray diffraction (XRD), scanning electron microscope (SEM), transmission electron microscope (TEM) and Brunauer-Emmett-Teller (BET). The effect of such unique porous structure on the electrochemical performance of TPO-NMS was extensively investigated in both organic and aqueous electrolytes. And the electrochemical properties of an aqueous lithium-ion battery based on TiP_2O_7 anode and $LiMn_2O_4$ cathode, including rate capacities and cycle performance, were also studied.

2 Experimental

2.1 Material synthesis

The precursor of TPO-NMS was prepared via a solid-state reaction. Stoichiometric amounts of Anatase TiO_2 (AR, Zhoushan New Material Co. Ltd., China), and $NH_4H_2PO_4$ (Sinopharm Chemical Reagent Co., Ltd., China) were mixed thoroughly with glucose (5 wt%) for 1 h, followed by the heat treatment at 600 °C for 5 h in air in the muffle furnace with heating rate of 5 °C/min. The resulting TiP_2O_7 precursor was reground to fine power by high-energy ball milling for 1 h and mixed with water to form slurry, which was then spray-dried for sphere-making. Schematic presentation of the synthesis process of carbon-coated TiP_2O_7 nanoporous microsphere is shown in Scheme 1.

2.2. Material characterization

XRD pattern was identified by a Bruker D8 X-ray diffractometer (Germany) using Cu Kα radiation (λ=1.5406 Å) with a step size of 0.02 between 10° to 80°. The refinements were carried out using the TOPAS software. SEM and TEM images were collected on Hitachi S-4800 (Japan) and Tecnai G2 F20 S-Twin (FEI, USA), respectively. Thermogravimetric (TG) measurements were characterized by Perkin-Elmer TGA 7 thermal analyzer (USA) recorded from 30 to 900 °C in O_2 atmosphere (60 mL/min). Nitrogen sorption isotherms were determined at 77 K using Quadrasorb SI Automated Surface Area and Pore Size Analyzer (USA). The samples were all degassed under vacuum at 300 °C for at least 3 h for the complete removal of contaminants and moisture. The specific surface area was calculated by the BET method. Pore size distribution was derived from the adsorption branch of isotherm using the Barrett-Joyner-Halenda (BJH) model. The tap density was measured using Quantachrome Autotap vibration densitometer (USA).

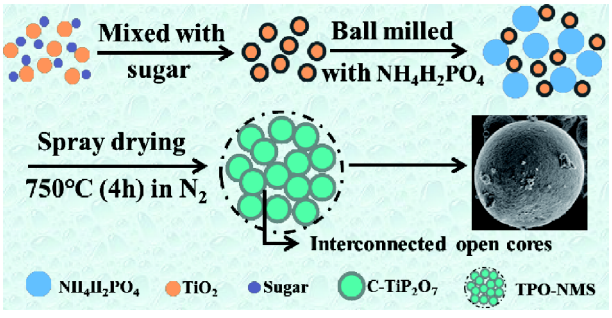

Scheme 1 Schematic presentation of the synthesis process of carbon-coated TiP_2O_7 nanoporous microsphere (TPO-NMS) (color online).

2.3 Electrochemical tests

The working electrode was prepared by compressing the mixture of 80 wt% active material (TPO-NMS), 10 wt% conducting agent (acetylene black) and 10 wt% binder (polytetrafluoroethylene, PTFE) into an uniform film electrode. After dried at 120 °C for at least 6 h, the electrode was pressed onto stainless steel mesh (10 MPa) through a manual hydraulic press (Carver, Inc., USA). The typical mass load of the active material of the working electrode is 2–3 mg/cm^2. The electrochemical tests in aqueous electrolyte were characterized using a three-electrode system equipped with an activated carbon counter electrode and a saturated calomel reference electrode (SCE, 0.242 V vs. NHE). A full cell consisting of TPO-NMS anode and $LiMn_2O_4$ cathode was also assembled. The mass ratio of anode and cathode was optimized to be 1:1. All the measurements were conducted in 1 M Li_2SO_4 solution as electrolyte under nitrogen atmosphere and performed on the HOKUTO DENKO Battery Charge/Discharge System HJ Series (Japan). For the electrochemical tests in organic electrolyte, the fabrication of working electrode was same to that conducted in aqueous electrolyte except the current collector which was changed to aluminum mesh. The electrode was dried at 80 °C under vacuum for 12 h before being assembled CR2016-type coin cells with the combination of working electrode/separator/metallic lithium counter electrode in an argon-filled glove box. The organic electrolyte used 1 M $LiPF_6$ solved in the mixture of ethylene carbonate (EC), dimethyl carbonate (DMC) and ethyl methyl carbonate (EMC) (1:1:1 by volume). The cell was galvanostatically cycled from 1.5 to 3.5 V (vs. Li/Li$^+$) on LAND CT2001A Battery Cycler (Wuhan Co. Ltd., China).

3 Results and discussion

Figure 1 shows the XRD patterns of TPO-NMS sample. Through the Rietveld refinement, all the sharp reflections can be indexed to the reference pattern (JCPDS #38-1468) with *Pa*3 space group and unit cell dimension a=23.6342 Å. As listed in Table 1, the value of χ^2-factor close to 1 indicates the consistency of experimental and calculated patterns. All the results including lattice parameters and atoms site occupancy are well agreement with other reports on the crystal structure of TiP_2O_7 [20,21,27,28]. However, there is no carbon observed in the pattern of TPO-NMS, which is most likely due to the amorphous structure or small amount of carbon [29]. However, the TG analysis shown in Figure 2 validates the presence of carbon. The content of carbon in TPO-NMS sample is approximately 5 wt%, based on the obvious weight loss from the TGA curve between 400 and 750 °C.

SEM images of the TPO-NMS sample are shown in Figure 3. Figure 3(a) displays the morphology of spherical particle with the diameter of 20 μm, which is aggregated by average primary nanoparticles of about 100 nm, as shown in the magnified image (Figure 3(b)). In order to observe the internal morphology of TPO-NMS microsphere, cross-sectional SEM images of an individual spherical particle were obtained through cutting the prepared electrode film in liquid nitrogen. As shown in Figure 3(c, d), its interior structure shows the similar morphology composed of nanosized particles. Additionally, numerous pores can be clearly observed which are generated by the aggregation of the primary particles, facilitating the deep penetration of electrolyte. To study the distribution of Ti, P, O and C elements in the secondary microspheres, the EDX elementary analysis was performed. The results in Figure 4 displays that the distribution of C elements is as uniform as Ti, P, O elements, indicating that this feasible synthesis process is in favor of the evenly distribution of carbon in the secondary particles.

Figure 5 displays the TEM and HRTEM images of TPO-NMS sample. As seen in Figure 5(b), a carbon layer with the thickness of ca. 6 nm evenly coats on the surface of primary

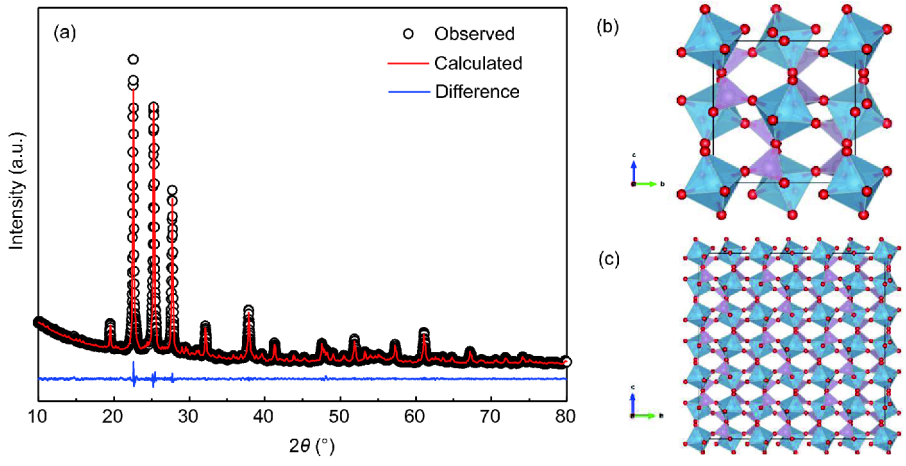

Figure 1 (a) Rietveld refinement of the XRD pattern of TPO-NMS sample; (b, c) the corresponding structures of TiP_2O_7 (color online).

Table 1 Crystallographic parameters for the TiP_2O_7 phase based on the Rietveld refinement of the XRD data

Parameters	data
Radiation	X-ray (Bruker D8 Advance X)
Crystal system	Cubic
Space group	*Pa*3
Lattice parameters	$a=b=c=23.63094$ Å, $\alpha=\beta=\gamma=90°$
Cell volume	13196.03 Å^3
λ	1.5406 Å
R_{wp} a)	5.365%
R_p a)	3.758%
χ^2 a)	1.4276

a) $R_{wp}=\sum \omega(I_0-I_C)^2 / \sum(\omega I_0^2)^{1/2}$; $R_p=\sum |I_0-I_C| / \sum I_C$; $\chi^2=\sum_\omega (I_0-I_C)^2 / \sum(N_{obs}-N_{var})$.

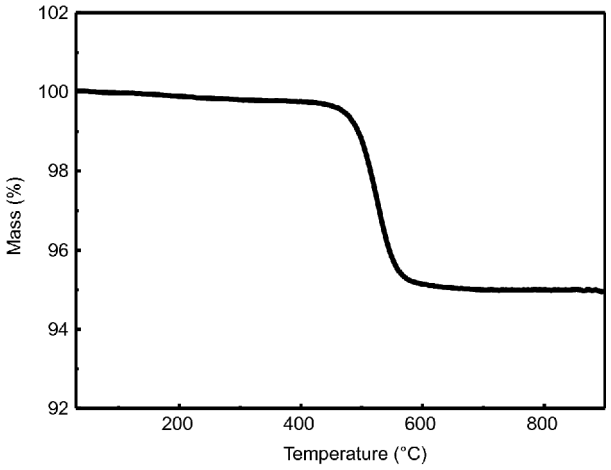

Figure 2 TG curve of the TPO-NMS.

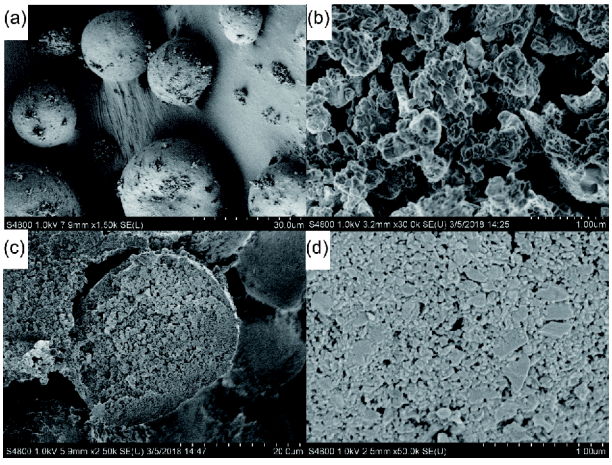

Figure 3 SEM images of TPO-NMS for (a) the secondary microsphere and (b) primary nanoparticles; (c) cross-section SEM image of one single secondary microsphere and (d) its magnified image.

particles. Associated with the EDX pattern, it testifies that carbon was completely and uniformly coated on TiP_2O_7 particles. The carbon coating coming from the carbonization

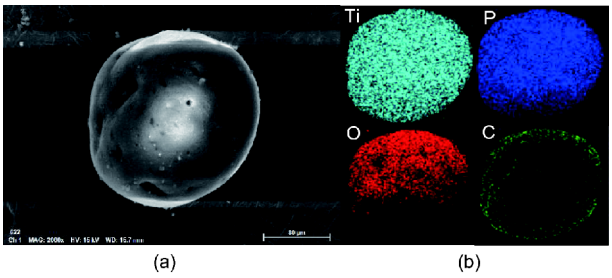

Figure 4 (a) SEM image of TPO-NMS for the one single secondary microsphere and (b) EDX elemental mapping of Ti, P, O and C elements (color online).

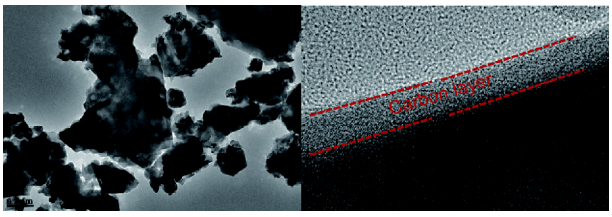

Figure 5 TEM images of TPO-NMS (color online).

of glucose suppresses the aggregation of primary TiP_2O_7 particles during the process of high-temperature calcination, effectively restricting the particle size on nanoscale. At the same time, it forms a conductive network within the material, greatly accelerating the electron transportation and improving the electronic conductivity of TPO-NMS [24,25].

The existence of pores in TPO-NMS sample is confirmed by the nitrogen sorption measurement. As shown in Figure 6, nanopores between 30 and 40 nm resulting from the agglomeration of nanoparticles identify the nanoporous structure. Combined with the SEM and TEM images above, numerous nanopores are well distributed in the material from surface to interior. Such interconnected pore structure provides many open channels for the penetration of electrolyte and a consequent enhancement of rate performance [30]. What's more, the sample has a small BET surface area of 8.587 m^2/g. The tap density was 0.77 g/mL. Compared to the discrete nano-sized counterparts, the smaller surface area predicts the high tap density and volumetric energy density, meeting the coating requirements of electrode materials in the practical large-scale production.

The electrochemical measurements of TPO-NMS were firstly conducted in organic electrolyte via a coin cell. Figure 7(a) depicts the typical charge/discharge curve of TPO-NMS in range of 0.5–1.7 V at a current density of 0.2 A/g. It displays the expected voltage plateau at 2.6 V, which is related to the Ti^{3+}/Ti^{4+} redox couple [31–33]. The electrode delivers a capacity of 81 mA h/g calculated on the mass of electrode active materials. Figure 7(b) shows the cycling performance and coulombic efficiency of TPO-NMS sample at 0.1 A/g. After 1000 cycles, it demonstrates good cycling stability with capacity maintenance of 88% and the average capacity

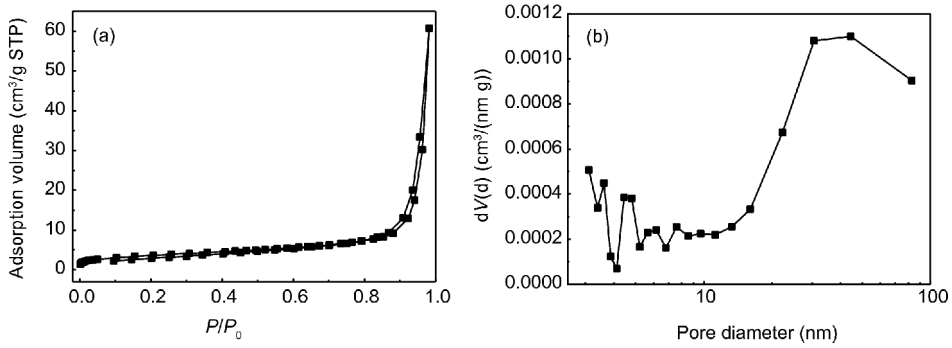

Figure 6 (a) N_2 sorption isotherm and (b) pore size distribution of TPO-NMS sample.

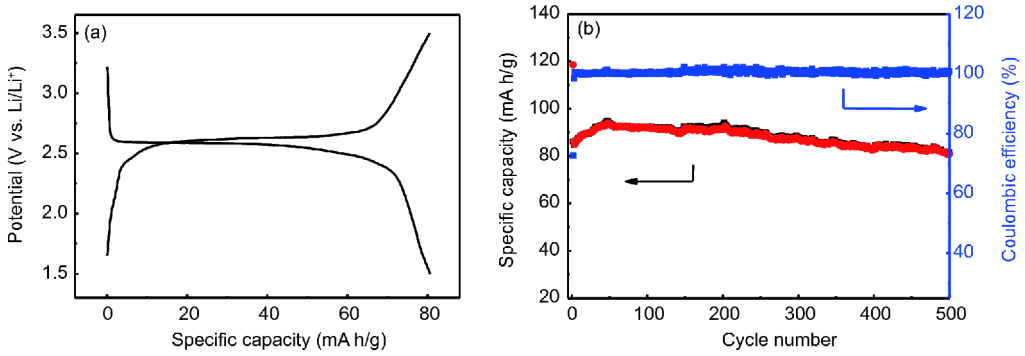

Figure 7 (a) Charge/discharge curve of TPO-NMS at 0.2 A/g between 1.5 and 3.5 V in organic electrolyte; (b) cycling performance of TPO-NMS at 0.1 A/g in organic electrolyte (color online).

fading of 0.024% for each cycle. Although the coulombic efficiency is only 72.6% in the first cycle, it rapidly grows to 98.5% in the second cycle and remains steady close to 100% in the subsequent cycles. To our best knowledge, such electrochemical performance can compete with that of other reported TiP_2O_7 anode materials for traditional lithium-ion batteries (as summarized in Table 2) [33–35]. This could be rationally contributed to the synthetic effects of smaller surface area and all-round nanometers-thick carbon layer which effectively impede the interfacial side reactions.

With the suitable Li-ion insertion potential of −0.63 V (vs. SCE) in neutral electrolyte before hydrogen evolution, TiP_2O_7 can be reasonably considered as a potential anode candidate for aqueous lithium-ion batteries. The intercalation potential of TiP_2O_7 has been extensively compared with several common anode materials like $LiTi_2(PO_4)_3$ and activated carbon (AC) through the linear scan voltammetry in our previous report [20]. The electrochemical performance of TPO-NMS in aqueous electrolyte was systemically studied. Figure 8(a) presents its rate capacity at different current rates from 0.1 to 10 A/g in the potential window of −0.8–0 V in 1 M Li_2SO_4 solution under N_2 atmosphere. The three-electrode cell firstly discharged at 0.1 A/g and then gradually grew to 10 A/g with each rate maintaining for 10 cycles. The TPO-NMS sample delivers a capacity of 90 mA h/g at 0.1 A/g, which is significantly higher than previously reported TiP_2O_7 [7,24,25]. Even at a high current rate of 10 A/g, namely 72 s per cycle, the electrode could still retain 50% capacity (vs. 0.1 A/g). This improved rate performance may be elucidated from the following aspects: (1) the uniform carbon coating on almost each nanoparticle constructs a conductive network inside and out, dramatically suppressing the aggregation of TiP_2O_7 particles and greatly improving the electronic conductivity; (2) nanoparticles to some extent shorten the lithium-ion diffusion pathways. What's more, such intricate porous structure favors the intraparticle full penetration of the electrolyte [20,25].

The cycling performance of TPO-NMS was also extensively studied at 0.5 A/g rate (Figure 8(b)) under N_2 atmosphere. After 500 cycles, it exhibits excellent cycling stability by delivering a capacity of 85 mA h/g with the capacity retention of 90%, namely, an average capacity decay of 0.02%. Generally, the TPO-NMS composite shows improved rate performance relative to other TiP_2O_7 composites and comparable cycling stability relative to similar non-aqueous systems using TiP_2O_7 as anode material [31–33].

Considering its satisfied electrochemical performance in both aqueous and organic electrolyte, an aqueous full cell that consists of a TPO-NMS anode and a $LiMn_2O_4$ cathode with the balancing mass ratio of 1:1 was assembled. The charge/discharge profiles of the individual electrodes of TPO-NMS/$LiMn_2O_4$ and the system is shown in Figure 9.

Table 2 Comparison of electrochemical performance of TiP_2O_7 composites synthesized through different process in organic electrolytes

Composition	Synthesis method	Voltage (V)	Current density	Capacity (mA h/g) (cycle number)	Capacity retention
Submicro-TPO [22]	Liquid-assisted method (900 °C-6 h in air)	2.0–3.4	15 mA/g	94(100)	76.12%
Nano-TPO [35]	Urea assisted combustion synthesis (900 °C-6 h in air)	2.0–3.4	15 mA/g	69(100)	87.0%
Planar TPO electrode [34]	Plasma-enhanced atomic layer deposition process	2.3–3.2	100 mA/g	120(100)	97.8%
Low temperature TPO [23]	Low temperature synthesis (800 °C-2 h)	1.5–3.5	5 mA/g	120(100)	75%
Flower-like TPO/C [33]	Solvothermal method (750 °C-4 h in N_2)	1.5–3.5	200 mA/g 600 mA/g 1000 mA/g	123(200) 90(400) 84(100)	93.2% 94.4% 98.4%
TPO/$Li_{2.6}Co_{0.4}N$ [36]	Co-precipitation method (600 °C-3 h in air)	0.02–1.5	0.4 mA/cm^2	647.54(20)	98%
Ti_3O_5/TPO@MPCNFs [37]	Electrospinning, sol-gel ripening	0.001–3.0	50 mA/g	713.3/509.3(100)	52.5%
TPO/EG [20]	Liquid-assisted method (750 °C-5 h in Ar)	1.5–3.5	100 mA/g	75(500)	88%
TPO-NMS (our work)	Solid-phase combined with spray drying method	1.5–3.5	100 mA/g	81(500)	88%

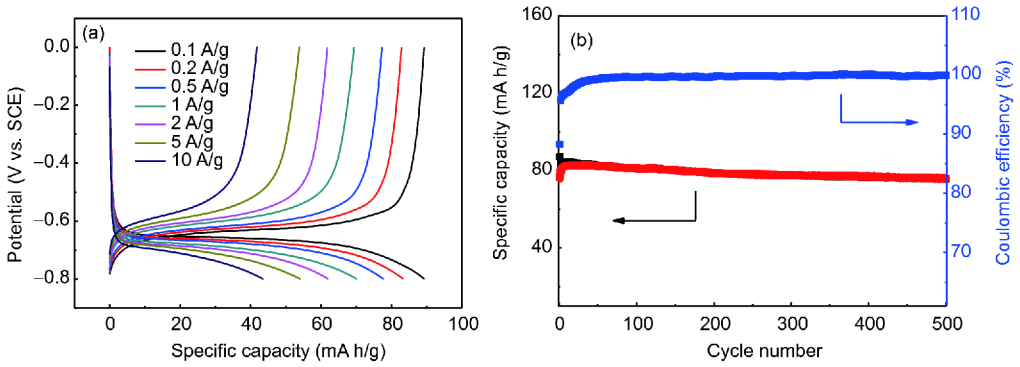

Figure 8 (a) Charge-discharge curves of TPO-NMS in 1 M Li_2SO_4 under nitrogen atmosphere within the voltage of −0.8 and 0 V at various current rates; (b) cycle performance of TPO-NMS in 1 M Li_2SO_4 solution at the rate of 0.5 A/g (color online).

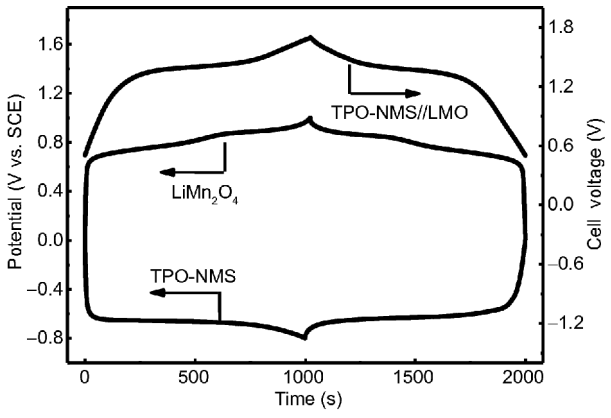

Figure 9 Typical charge/discharge curves of the individual electrode TPO-NMS and $LiMn_2O_4$ (vs. SCE) along with the voltage profile of the aqueous lithium-ion battery in the range of 0.5−1.7 V at a current rate of 0.2 A/g.

The cell cycled between 0.5 and 1.7 V at the current density of 0.2 A/g delivers a voltage plateau of 1.4 V with good reversibility, and exhibits an initial capacity of 45 mA h/g and a specific energy of 63 W h/kg based on the total weight of both electrode active materials.

The rate performance of TPO-NMS/$LiMn_2O_4$ full cell at different current rates is demonstrated in Figure 10(a, b). The current rates are calculated based upon the weight of TPO-NMS anode. The cell shows good rate capability with the capacities of 45, 43, 40, 36, 34, 30, 25 mA h/g at the current rates of 0.1, 0.2, 0.5, 1.0, 2.0, 5.0 and 10.0 A/g respectively. And 56% of capacity retention is maintained at the high rate of 10.0 A/g (vs. 0.1 A/g). Figure 10(c) elucidated the cycle life of the full cell. As observed, it can maintain 80% of capacity after 1000 cycles at 0.5 A/g. As compared in Table 2, this outperforms previous reported counterparts in the

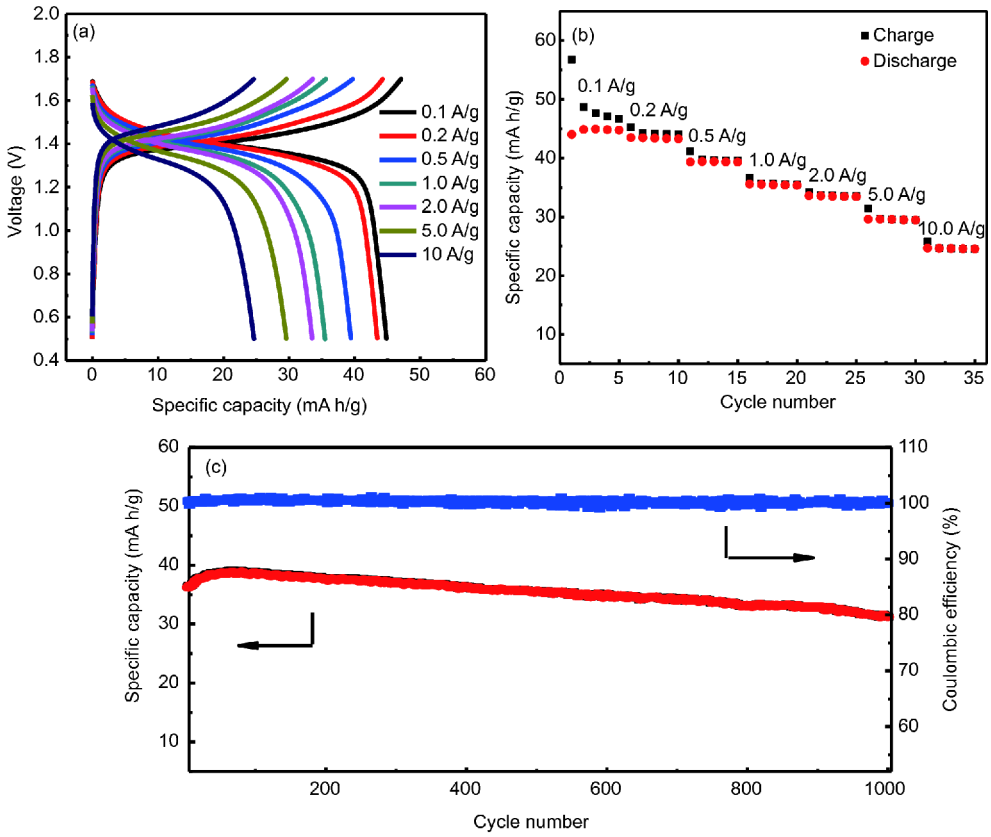

Figure 10 (a) Charge/discharge curves and (b) capacity retention plots of TPO-NMS//$LiMn_2O_4$ cell at different rates; (c) cycle performance of TPO-NMS//$LiMn_2O_4$ cell at 0.5 A/g for 1000 cycles (color online).

$LiMn_2O_4$/aqueous electrolytes/TiP_2O_7 system, 38% after 25 cycles at 0.1 C [7], 33% after 100 cycles at 2 C [38] and 85% after 100 cycles at 0.5 C [24]. Such enhanced rate performance and cycling stability fully demonstrate the advisable application of spray drying method and the possibility of TPO-NMS used as anode material for high power density aqueous lithium-ion batteries.

4 Conclusions

In the present work, we reported a facile way to mass-produce a carbon-coated TiP_2O_7 nanoporous microsphere (TPO-NMS) via solid state method combined with spray drying process. With the unique advantage of working potential (−0.6 V vs. SCE) before hydrogen evolution, TPO-NMS composite has been evaluated as anode material in both organic and aqueous electrolytes, in which the primary nanoparticles with uniform carbon coating and interconnected pore structure greatly improve its electrochemical properties. This anode displays a reversible capacity of 90 mA h/g at 0.1 A/g in 1 M Li_2SO_4 solution and still maintains 52% of the capacity at 10 A/g (vs. 0.1 A/g). Additionally, over 90% of capacity retention after 500 cycles at 0.2 A/g manifests the prominent cycling stability of TPO-NMS. Moreover, an aqueous battery TPO-NMS/1 M Li_2SO_4/$LiMn_2O_4$ exhibits a voltage plateau around 1.4 V with a specific energy of 63 W h/kg based on the weight of anode and cathode and demonstrates good rate performance as well as remarkable cycling stability with the capacity maintenance of 82% after 1000 cycles at 0.5 A/g. This ARLB is of great potential for EV/HEV and stationary energy storage applications. Moreover, the synthesis method presented here may renew interest in the fabrication of other electrode materials.

Acknowledgements This work was supported by the National Natural Science Foundation of China (21333002), and the National Key Research and Development Plan (2016YFB0901500).

Conflict of interest The authors declare that they have no conflict of interest.

1 Kim H, Hong J, Park KY, Kim H, Kim SW, Kang K. *Chem Rev*, 2014, 114: 11788–11827
2 Chang Z, Yang Y, Li M, Wang X, Wu Y. *J Mater Chem A*, 2014, 2: 10739–10755
3 Alias N, Mohamad AA. *J Power Sources*, 2015, 274: 237–251
4 Li W, Dahn JR, Wainwright DS. *Science*, 1994, 264: 1115–1118
5 Köhler J, Makihara H, Uegaito H, Inoue H, Toki M. *Electrochim Acta*, 2000, 46: 59–65
6 Wang H, Zeng Y, Huang K, Liu S, Chen L. *Electrochim Acta*, 2007, 52: 5102–5107
7 Wang H, Huang K, Zeng Y, Yang S, Chen L. *Electrochim Acta*, 2007, 52: 3280–3285

8 Wang G, Qu Q, Wang B, Shi Y, Tian S, Wu Y. *ChemPhysChem*, 2008, 9: 2299–2301
9 Wang GX, Zhong S, Bradhurst DH, Dou SX, Liu HK. *J Power Sources*, 1998, 74: 198–201
10 Wang Y, Chen L, Wang Y, Xia Y. *Electrochim Acta*, 2015, 173: 178–183
11 Wang Y, Luo J, Wang C, Xia Y. *J Electrochem Soc*, 2006, 153: A1425
12 Wang G, Fu L, Zhao N, Yang L, Wu Y, Wu H. *Angew Chem Int Ed*, 2007, 46: 295–297
13 Manickam M, Singh P, Thurgate S, Prince K. *J Power Sources*, 2006, 158: 646–649
14 He P, Liu JL, Cui WJ, Luo JY, Xia YY. *Electrochim Acta*, 2011, 56: 2351–2357
15 Wang Y, Yi J, Xia Y. *Adv Energy Mater*, 2012, 2: 830–840
16 Luo JY, Cui WJ, He P, Xia YY. *Nat Chem*, 2010, 2: 760–765
17 Luo JY, Xia YY. *Adv Funct Mater*, 2007, 17: 3877–3884
18 Li W. *J Electrochem Soc*, 1995, 142: 1742–1746
19 Wessells C, Huggins RA, Cui Y. *J Power Sources*, 2011, 196: 2884–2888
20 Wen Y, Chen L, Pang Y, Guo Z, Bin D, Wang Y, Wang C, Xia Y. *ACS Appl Mater Interfaces*, 2017, 9: 8075–8082
21 Patoux S, Masquelier C. *Chem Mater*, 2002, 14: 5057–5068
22 Hao Y, Wu C, Cui Y, Xu K, Yuan Z, Zhuang Q. *Ionics*, 2014, 20: 1079–1085
23 Senguttuvan P, Rousse G, Oró-Solé J, Tarascon JM, Palacín MR. *J Mater Chem A*, 2013, 1: 15284–15289
24 Li C, Sun X, Du Q, Zhang H. *Solid State Ion*, 2013, 249-250: 72–77
25 Wu W, Shanbhag S, Wise A, Chang J, Rutt A, Whitacre JF. *J Electrochem Soc*, 2015, 162: A1921–A1926
26 Zhang H, Zhou Y, Li C, Yang C, Zhu T. *J Mater Chem A*, 2016, 4: 13390–13394
27 Norberg ST, Svensson G, Albertsson J. *Acta Crystlogr C Cryst Struct Commun*, 2001, 57: 225–227
28 Sanz J, Iglesias JE, Soria J, Losilla ER, Aranda MAG, Bruque S. *Chem Mater*, 1997, 9: 996–1003
29 Hu S, Song Y, Yuan S, Liu H, Xu Q, Wang Y, Wang CX, Xia YY. *J Power Sources*, 2016, 303: 333–339
30 Liu J, Conry TE, Song X, Doeff MM, Richardson TJ. *Energy Environ Sci*, 2011, 4: 885–888
31 Rai AK, Gim J, Song J, Mathew V, Anh LT, Kim J. *Electrochim Acta*, 2012, 75: 247–253
32 Shi Z, Wang Q, Ye W, Li Y, Yang Y. *Microporous Mesoporous Mater*, 2006, 88: 232–237
33 Sun Y, Gai L, Zhou Y, Zuo X, Zhou J, Jiang H. *CrystEngComm*, 2014, 16: 10681–10691
34 Dobbelaere T, Mattelaer F, Roy AK, Vereecken P, Detavernier C. *J Mater Chem A*, 2017, 5: 330–338
35 Aravindan V, Reddy MV, Madhavi S, Mhaisalkar SG, Subba Rao GV, Chowdari BVR. *J Power Sources*, 2011, 196: 8850–8854
36 Rai AK, Lim J, Mathew V, Gim J, Kang J, Paul BJ, Kim D, Ahn S, Kim S, Ahn K, Kim J. *Electrochem Commun*, 2012, 19: 9–12
37 Teng D, Yu Y, Li P, Bai X, Yang X. *RSC Adv*, 2013, 3: 14237–14240
38 Sun K, Juarez DA, Huang H, Jung E, Dillon SJ. *J Power Sources*, 2014, 248: 582–587